Analytical Study of Performance Parameters of InGaN/GaN Multiple Quantum Well Solar Cell

Gaurav Siddharth, Vivek Garg, Brajendra S. Sengar, Ritesh Bhardwaj, Pawan Kumar, and Shaibal Mukherjee, *Senior Member, IEEE*

***Abstract*— An analytical study has been carried out to obtain the device performance parameters of InGaN/GaN-based multiple quantum well solar cell (MQWSC). Significant improvements are made upon the preexisting models reported in the literature for predicting device performance matrix for MQWSC. The American Society for Testing and Materials (ASTM) standards data sheets are utilized for attaining photon flux density instead of blackbody radiation formula. Furthermore, the photon flux density is utilized to evaluate the performance parameters of MQWSC and bulk p-i-n solar cell. Results suggest that by incorporating QWs in the intrinsic region ($x = 0.1$ in $In_xGa_{1-x}N$), ~27% increment in the conversion efficiency can be achieved as compared to that from the bulk solar cell. Moreover, the impact of operating temperature in the solar cell performance is also studied. The rise in temperature leads to an increase in short-circuit current density; however, open-circuit voltage and conversion efficiency decrease. A decrement of ~9.7% in the conversion efficiency of MQWSC is observed with the rise in temperature from 200 to 400 K as compared to ~11.6% decline in p-i-n solar cell.**

***Index Terms*— AM1.5G, American Society for Testing and Materials (ASTM), multiple quantum well solar cell (MQWSC), photon flux density.**

I. Introduction

InGaN alloy offers a great possibility for solar cell applications because its energy bandgap can be varied continuously from 0.7 to 3.4 eV, which can be utilized to cover almost the entire solar spectrum [1]. Apart from the direct and wide energy bandgap, it possesses the favorable photovoltaic properties such as high mobility, the low effective mass of carrier, and high absorption coefficient [2]. Various aspects such as optical and structural characteristics of InGaN alloy for the photovoltaic application are discussed by Jani *et al.* [2] and InGaN-based p-i-n and quantum well (QW) solar cells are also designed, in which InGaN is deployed as the active layer [3].

In the last few decades, the multiple QW solar cells (MQWSCs) have been studied extensively, where QWs are used in the intrinsic region of a p-i-n solar cell to enhance the conversion efficiency of the solar cell [4]. There is an efficiency limitation in the conventional solar cell, which originates from the tradeoff between a high-energy bandgap, which enhances the open-circuit voltage, and a low-energy bandgap, which boosts short-circuit current [5], [6]. However, this limitation can be avoided by utilizing MQWs in the intrinsic layer of the solar cell, as both the current and voltage performance parameters of the device can be controlled and optimized independently [7]. It is well known that the value of energy bandgap of the well material must be smaller than that of the p-i-n solar cell in order to have additional energy sub-band levels between conduction and valence bands [8]–[10]. The MQWSCs can also be used in the multijunction solar cells (MJSCs) for the efficient current matching of the top, middle, and bottom cells [11]. Different models have been proposed to understand the performance of the MQWSC [12]–[15]. Connolly *et al.* [12] have not considered capture and escape rates from the well and characterized the dark current in terms of the QW density of states. A model including the escape, capture, and recombination of the photoexcited carriers in QWs was proposed by Ramey and Khoie [13] in which an improved conversion efficiency is presented by inserting MQWs in the depletion region of p-i-n solar cell. Aperathitis *et al.* [14] have examined the tunneling current contribution to the photocurrent at various temperatures on AlGaAs/GaAs MQWSC. Anderson [15] developed an ideal model for MQWSC, incorporating carrier generation and recombination in the QWs, and discussed the qualitative analysis of MQWSC performance.

In this work, a physics-based analytical model is presented to obtain device performance parameters of the InGaN/GaN MQWSCs and p-i-n solar cells. An extensive discussion on the temperature dependence of these parameters is studied. The conversion efficiency variation with the number of QWs in MQWSC is also studied. Significantly, the American Society for Testing and Materials (ASTM) standards data sheets and spectral irradiance are utilized for attaining photon flux density instead of blackbody radiation formula used in other published literature [16], [17]. Furthermore, this photon flux density will be used for the calculation of performance parameters of the device.

II. Model Development

The solar energy spectra for space and terrestrial application referred to as AM0, AM1.5G, and AM1.5D are based on ASTM standards [18]–[20]. In the developed models, the device performance parameters such as short-circuit

Manuscript received February 1, 2019; revised May 6, 2019 and May 22, 2019; accepted May 31, 2019. The review of this paper was arranged by Editor B. Hoex. *(Corresponding author: Shaibal Mukherjee.)*

The authors are with the Hybrid Nanodevice Research Group (HNRG), Electrical Engineering, IIT Indore, Indore 453552, India (e-mail: phd1601102010@iiti.ac.in; phd1401102015@iiti.ac.in; phd1401102005@iiti.ac.in; phd1501102012@iiti.ac.in; phd1701202002@iiti.ac.in; shaibal@iiti.ac.in).

Color versions of one or more of the figures in this paper are available online at http://ieeexplore.ieee.org.

Digital Object Identifier 10.1109/TED.2019.2920934

current density, open-circuit voltage, and energy conversion efficiency are studied for different indium compositions (x = 0.1, 0.2, and 0.3) in $In_xGa_{1-x}N$ (intrinsic region) and at different temperatures. Despite the fact that higher indium composition leads to a much better spectral overlap, it is limited to 0.3 in this work, as the higher composition reduces the crystalline quality leading to a larger loss of photogenerated charge carriers [21]. In this work, the data sheets from the ASTM standard are used, to ascertain the photon flux density [22] instead of the blackbody radiation formula, which differs from the actual solar energy spectra. Models have been developed for two different device structures [p-i(bulk)-n and p-i(MQWs)-n solar cells].

A. For p-i(Bulk)-n Solar Cell

The illuminated current density versus voltage (J–V) characteristics of the p-i-n solar cell is described by the Shockley solar cell equation [15], [23]

$$J_{\mathrm{Bu}}(V) = J_s[\exp(V/V_t) - 1] - J_{\mathrm{Ge}} + J_{\mathrm{Re}} \tag{1}$$

where V is the terminal voltage, V_t is the thermal voltage, J_s is the reverse saturation current density (the term including J_s represents the ideal recombination current from the diffusion and recombination of electrons and holes), J_{Ge} and J_{Re} are the superimposed current densities corresponding to carrier generation (because of illumination by solar spectra) and recombination in the intrinsic region, respectively. For p-i-n solar cell, the generation and recombination current density terms can be written as in (2) and (3) [15], [23]

$$J_{\mathrm{Ge}} = qt_i[G_{\mathrm{BuO}} + G_{\mathrm{BuT}}] \tag{2}$$

$$J_{\mathrm{Re}} = qt_i R_{\mathrm{Bu}} = qt_i B_{\mathrm{Bu}} n_{\mathrm{iBu}}^2 \exp(V/V_t) \tag{3}$$

where t_i is the intrinsic region thickness and G_{BuO} and G_{BuT} are the optical and thermal generation rates, respectively, throughout the intrinsic region, R_{Bu} is the average recombination rate in the intrinsic region, B_{Bu} is the barrier recombination coefficient, n_{iBu} is the equilibrium intrinsic carrier concentration. Since $G_{\mathrm{BuT}} = B_{\mathrm{Bu}} n_{\mathrm{iBu}}^2$, and by substituting the equation of J_{Ge} and J_{Re} in (1), J–V characteristics of the p-i-n solar cell are

$$J_{\mathrm{Bu}}(V) = J_s(1+\beta_1)[\exp(V/V_t) - 1] - qt_i G_{\mathrm{BuO}} \tag{4}$$

where the factor β_1 describe the contribution of the current required to feed radiative recombination in the intrinsic region at equilibrium and is given as

$$\beta_1 = \frac{qt_i B_{\mathrm{Bu}} n_{\mathrm{iBu}}^2}{J_s}. \tag{5}$$

The short-circuit current density is obtained by replacing $V = 0$ in (4) and is given as

$$J_{\mathrm{scBu}} = -qt_i G_{\mathrm{BuO}} = -q[f_2 N_{\mathrm{ph}}(E > E_{\mathrm{Bu}}) + N_{\mathrm{ph}}(E = E_{\mathrm{Bu}})]. \tag{6}$$

The term $N_{\mathrm{ph}}(E > E_{\mathrm{Bu}})$ is the net photon flux density corresponding to the energies greater than E_{Bu}, $N_{\mathrm{ph}}(E = E_{\mathrm{Bu}})$ is the net photon flux density corresponding to the energy E_{Bu}, and f_2 is the fraction of the light absorbed whose energies are above the energy bandgap [24]. The open-circuit voltage is obtained by evaluating $J_{\mathrm{Bu}}(V) = 0$ in (4) and is given by

$$V_{\mathrm{ocBu}} = V_t \ln\left[\frac{J_s(1+\beta_1) - J_{\mathrm{scBu}}}{J_s(1+\beta_1)}\right]. \tag{7}$$

The device performance parameter, which describes the quality of the J–V curve, is the fill factor (FF) and is defined as [24], [25]

$$\mathrm{FF} = \frac{V_{\mathrm{mBu}} J_{\mathrm{mBu}}}{V_{\mathrm{ocBu}} J_{\mathrm{scBu}}} \tag{8}$$

where V_{mBu} and J_{mBu} are the voltage and current density, respectively, corresponding to the maximum power density point on the J–V characteristic of the solar cell, at which it has the maximal power density. The operating regime of the solar cell in which it delivers the power is in the range from 0 to V_{oc}. The power density of the solar cell is given by $P = JV$ [25]. The voltage V_{mBu} is obtained by the derivation of power density P with respect to voltage V and then equating $(\partial P/\partial V) = 0$ [26]–[28]. The final equation that is used to obtained V_{mBu} by the iteration method is

$$\exp\left(\frac{V_{\mathrm{ocBu}}}{V_t}\right) - \exp\left(\frac{V_{\mathrm{mBu}}}{V_t}\right)\left[1 + \frac{V_{\mathrm{mBu}}}{V_t}\right] = 0. \tag{9}$$

Similarly, the value of J_{mBu} is obtained by the derivation of power density P with respect to current density J and then equating $(\partial P/\partial J) = 0$. Therefore, the final iterative equation which is used to obtain J_{mBu} is

$$\frac{J_{\mathrm{mBu}}}{J_{\mathrm{mBu}} - J_{\mathrm{scBu}} + J_s(1+\beta_1)} + \ln\left[\frac{J_{\mathrm{mBu}} - J_{\mathrm{scBu}} + J_s(1+\beta_1)}{J_s(1+\beta_1)}\right] = 0. \tag{10}$$

The energy conversion efficiency (η) of the solar cell is given by [25]

$$\eta = \frac{V_{\mathrm{oc}} J_{\mathrm{sc}} \mathrm{FF}}{P_{\mathrm{in}}} \times 100\% \tag{11}$$

where $P_{\mathrm{in}} = 100\mathrm{mW/cm}^2$, as is described by the AM1.5 spectrum, is the irradiance of the incident light.

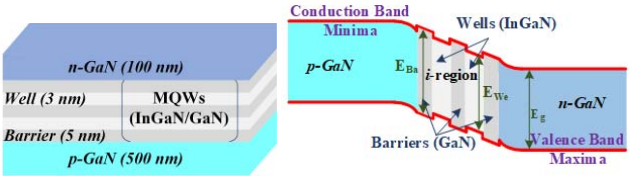

Fig. 1. Structure of QWSC with its corresponding energy band diagram.

B. For p-i(MQWs)-n Solar Cell

The MQWSC is basically a p-i-n solar cell containing multiple numbers of QWs in the intrinsic region (active region). The basic structure of QWSC is shown in Fig. 1 with its corresponding band diagram. The MQWSC structure consists of QW material of energy bandgap E_{We} less than that of the barrier material having energy bandgap of E_{Ba}. With the modification in (4), the illuminated J–V characteristics of

the MQWSC including the generation and recombination in the well and barrier region are described by

$$J_{\mathrm{QW}}(V) = J_s(1+r\beta_1)[\exp(V/V_t)-1] - qt_i[f_1 G_{\mathrm{WeO}} + (1-f_1)G_{\mathrm{BaO}}] \quad (12)$$

where $r = 1+f_1[\gamma_1\gamma_2^2\exp(\Delta E/kT-1)]$ includes the enhancement in the dark recombination current because of the presence of the QWs in the intrinsic region, $\gamma_1 = B_{\mathrm{We}}/B_{\mathrm{Ba}}$ is the recombination coefficient enhancement factor, $\gamma_2 = g_{\mathrm{We}}/g_{\mathrm{Ba}}$ is the effective volume densities of states enhancement factor, and $\Delta E = E_{\mathrm{Ba}} - E_{\mathrm{We}}$.

The short-circuit current density for the MQWSC is obtained by substituting $V = 0$ in (12) and is given as

$$\begin{aligned} J_{\mathrm{scQW}} &= -qt_i[f_1 G_{\mathrm{WeO}} + (1-f_1)G_{\mathrm{BaO}}] \\ &= -q[f_w N_{\mathrm{ph}}(E_{\mathrm{Ba}} > E_{\mathrm{We}}) + (1-f_w)N_{\mathrm{ph}}(> E_{\mathrm{Ba}})] \end{aligned} \quad (13)$$

where $N_{\mathrm{ph}}(E_{\mathrm{Ba}} > E_{\mathrm{We}})$ is the net photon flux density corresponding to the energies between E_{Ba} and E_{We} and $N_{\mathrm{ph}}(> E_{\mathrm{Ba}})$ is defined similarly as for the bulk solar cell. Now, by substituting $J_{\mathrm{QW}} = 0$ in (12), the open-circuit voltage can be obtained and is given as follows:

$$V_{\mathrm{ocQW}} = V_t \ln\left[\frac{J_s(1+r\beta_1) - J_{\mathrm{scQW}}}{J_s(1+r\beta_1)}\right]. \quad (14)$$

V_{mQW} and J_{mQW} are the voltage and current density, respectively, corresponding to the maximum power density point on the J–V characteristic of the MQWSC and can be obtained in the similar way as it is obtained for the p-i-n solar cell. The final expression used for getting them is as follows:

$$\exp\left(\frac{V_{\mathrm{ocQW}}}{V_t}\right) - \exp\left(\frac{V_{\mathrm{mQW}}}{V_t}\right)\left[1+\frac{V_{\mathrm{mQW}}}{V_t}\right] = 0 \quad (15)$$

$$\frac{J_{\mathrm{mQW}}}{J_{\mathrm{mQW}} - J_{\mathrm{scQW}} + J_s(1+r\beta_1)} + \ln\left[\frac{J_{\mathrm{mQW}} - J_{\mathrm{scQW}} + J_s(1+r\beta_1)}{J_s(1+r\beta_1)}\right] = 0. \quad (16)$$

C. Basic Parameter Equation

The dependence of the energy bandgap of the $\mathrm{In}_x\mathrm{Ga}_{1-x}\mathrm{N}$ alloy on the indium composition is obtained by using Vegard's law and can written as [29]

$$E_g(\mathrm{In}_x\mathrm{Ga}_{1-x}N) = xE_g(\mathrm{In}N) + (1-x)E_g - bx(1-x) \quad (17)$$

where b is the bowing parameter whose value for $\mathrm{In}_x\mathrm{Ga}_{1-x}\mathrm{N}$ is 1.43. The variation of the energy bandgap with the temperature can be described by the expression given by Varshni [30]

$$E_g(T) = E_{\mathrm{g0}} - \frac{\beta_2 T^2}{T+\beta_3} \quad (18)$$

where T is the absolute temperature, E_{g0} is the energy bandgap at 0° K, and β_2 and β_3 are material-dependent parameters.

The reverse saturation current density (J_s) is given by

$$J_s = qn_i^2\left(\frac{D_p}{L_p N_D} + \frac{D_n}{L_n N_A}\right) \quad (19)$$

where D_p and D_n are the diffusion constants for holes and electrons, respectively, and given by Einstein relation, L_p and L_n are the diffusion length for holes and electrons, respectively, and given by $L = \sqrt{D\tau}$, where τ is the minority carrier lifetime and N_A and N_D are the acceptor and donor concentrations.

The general absorption coefficient valid for all dimensional (D) materials for free carriers is given in [31]

$$\alpha(\omega) = \alpha_0^D \frac{\hbar\omega}{E_1}\left(\frac{\hbar\omega - E_g - E_0^D}{E_1}\right)^{\frac{D-2}{2}} \times \Theta\left(\hbar\omega - E_g - E_0^D\right)A(\omega) \quad (20)$$

where $\Theta(x)$ is the Heavyside function, $A(\omega)$ is the band-filling factor, $E_0^D = \{\hbar^2\pi^2(3-D)\}/\{2m_r L_c^2\}$ is the zero-point energy, and the scaling parameters, $E_1 = \hbar^2/(2m_r a^2)$ and $a = \hbar^2\varepsilon_0/(q^2 m_r)$. Most of the photon absorption occurs over the penetration depth, $\delta = 1/\alpha$. The thickness of the absorption material depends on the penetration depth and the diffusion coefficient of hole and electron by the following relation: diffusion lengths (L_p and L_n) > absorber thickness > penetration depth (δ) [32].

The spectral photon flux density is calculated from the spectral irradiance ($E(\lambda)$) by using the expression [22], [33]

$$N_{\mathrm{ph}}(\lambda) = E(\lambda)\frac{\lambda}{\mathrm{hc}} = 5.034\times10^{14}E(\lambda)\lambda \quad (21)$$

where h is Planck's constant and c is the speed of light. The photon flux density is useful for calculating the theoretical number of photons that can be collected as a function of photovoltaic material bandgaps [22], [25].

III. Results and Discussions

Based on the analytical expressions derived above, the performance of both p-i-n and MQWs solar cells has been evaluated. The J–V characteristics and device performance parameters of both the structures and their variation with temperature are illustrated in this section.

A. For p-i(bulk)-n Solar Cell

Fig. 2 demonstrates the dark and illuminated J–V characteristics of the p-i-n solar cell with different indium composition (x) of $\mathrm{In}_x\mathrm{Ga}_{1-x}\mathrm{N}$ in the intrinsic region. The higher value of x in $\mathrm{In}_x\mathrm{Ga}_{1-x}\mathrm{N}$ alloy reduces the energy bandgap of the intrinsic layer, because of which, J_{scBu} increases as a result of the increase in the carrier generation; however, V_{ocBu} decreases as a result of the increase in the carrier recombination [13], [34], [35]. Table I lists the performance parameters of the p-i-n solar cell for different x. As can be observed from Table I, the increase in J_{scBu} with increasing x is larger as compared to the reduction in V_{ocBu}, consequently leading to the overall rise in the value of η. η increases by ~37% and ~56% for $x = 0.2$ and 0.3, respectively, as compared to that for $x = 0.1$. Therefore, the increase in x in the intrinsic region of the p-i-n solar cell enhances the solar cell conversion efficiency.

As the temperature of operation has a significant impact on solar cell performance, its effects on p-i-n solar cell performance parameters have been studied and are depicted in Fig. 3. With the rise in temperature, the energy bandgap decreases as depicted by (18), and because of that extra lower energy

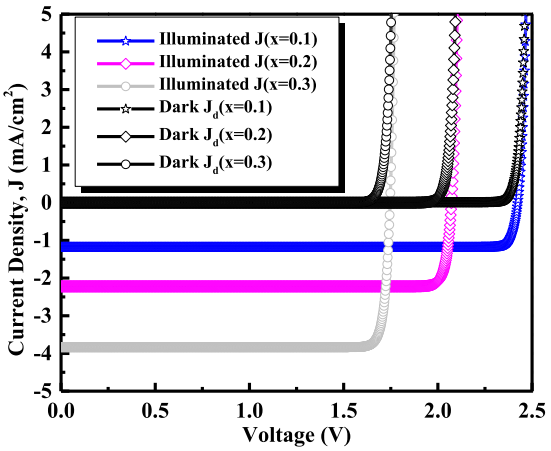

Fig. 2. *J–V* characteristics for p-i-n solar cell with different indium compositions (x) of $In_xGa_{1-x}N$ in the intrinsic region.

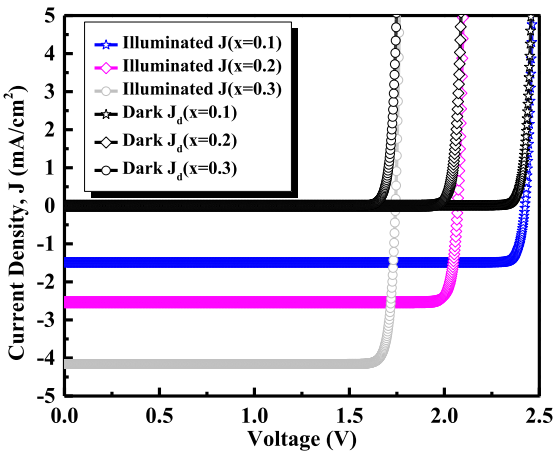

Fig. 4. *J–V* characteristics for MQWSC with different indium compositions (x) of $In_xGa_{1-x}N$ in the intrinsic region.

TABLE I
PERFORMANCE PARAMETERS OF p-i-n SOLAR CELL WITH DIFFERENT INDIUM COMPOSITIONS OF $In_xGa_{1-x}N$

Parameters	$x = 0.1$	$x = 0.2$	$x = 0.3$
J_{sc} (mA/cm^2)	1.18	2.22	3.84
V_{oc} (V)	2.42	2.07	1.75
η (%)	2.69	4.28	6.18

TABLE II
PERFORMANCE PARAMETERS OF MQWS SOLAR CELL WITH DIFFERENT INDIUM COMPOSITIONS OF $In_xGa_{1-x}N$

Parameters	$x = 0.1$	$x = 0.2$	$x = 0.3$
J_{scQW} (mA/cm^2)	1.50	2.53	4.16
V_{ocQW} (V)	2.43	2.07	1.74
η (%)	3.42	4.89	6.69

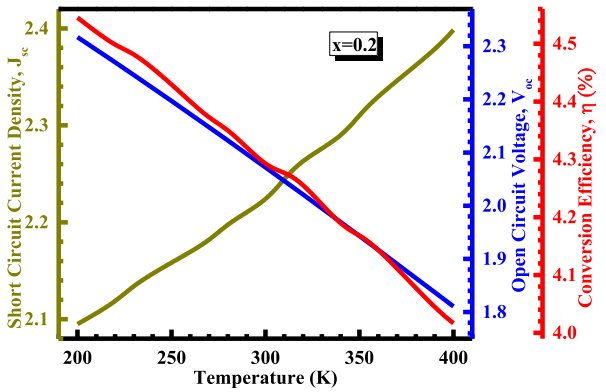

Fig. 3. Temperature-dependent short-circuit current density, open-circuit voltage, and conversion efficiency of p-i-n solar cell.

photons will be absorbed, which results in the increment of J_{scBu}. As expressed in (7), V_{ocBu} is determined by both J_{scBu} and J_s, however, the influence of the increase in J_s is more as compared to the increase in J_{scBu} with the increasing temperature, leading to the overall decrement of V_{ocBu} [36] and it follows approximately the linear curve [25]. As the temperature increases from 200 to 400 K, the larger reduction of V_{ocBu} (~28 %) as compared to the minor enhancement in the value of J_{scBu} (~13 %) eventually leads to the reduction in the value of η (~13 %) [5], [25], indicating that η has a negative temperature coefficient. Therefore, it is concluded that the rise in temperature leads to the reduction of the conversion efficiency.

B. For p-i(MQWs)-n Solar Cell

In this section, a discussion is presented on the results obtained for the MQWSC. The QW structure consists of GaN and InGaN as barrier and well materials, respectively, in the intrinsic region of the p-i-n structure, whereas the p- and n-regions are based on GaN material.

Fig. 4 exhibits the dark and illuminated *J–V* characteristics of the MQWSC that consists of 20 wells of thickness 3 nm each with different indium concentration in $In_xGa_{1-x}N$ and 21 barriers each having 5 nm thickness. The device performance parameters are summarized in Table II. The indium composition (x) of $In_xGa_{1-x}N$ in well has the similar effects on the *J–V* characteristics of MQWSC and its parameters as that for the p-i-n solar cell. As x increases from 0.1 to 0.3, J_{scQW} increases by ~41% and ~64%, respectively, whereas V_{ocQW} decreases by ~17% and ~39%, respectively, leading to the overall increment in η by ~30% and ~27%, respectively.

In Fig. 5, temperature-dependent device performance parameters of the MQWSC are exemplified. With the rise in temperature from 200 to 400 K, J_{scQW} increases from 2.37 to 2.77 mA/cm^2, respectively, and V_{ocQW} decreases from 2.32 to 1.81 V, respectively, due to which η decreases from 5.15% to 4.65%, respectively. The reason behind the increment in J_{scQW} and decrement in both V_{ocQW} and η is similar as explained for p-i-n solar cell; however, the impact of temperature on MQWSC is less as compared to that on p-i-n solar cell because the carrier escape mechanism in the QWs is mainly thermally activated and also MQW structure has better absorption properties than those of bulk materials [5], [37].

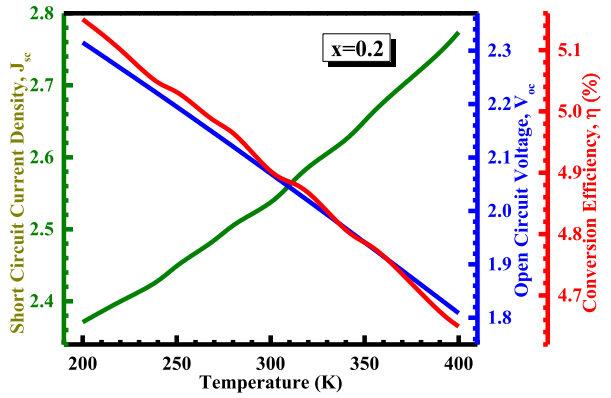

Fig. 5. Temperature-dependent variation of short-circuit current density, open-circuit voltage, and conversion efficiency for MQWSC.

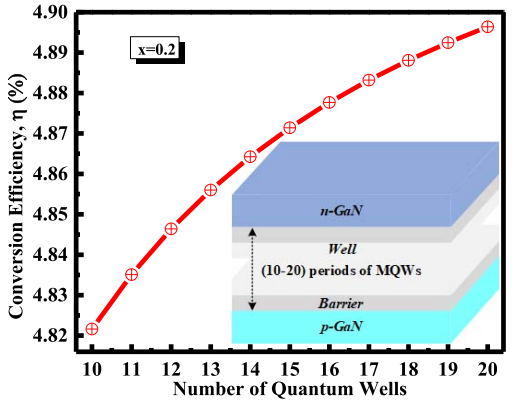

Fig. 6. Variation of conversion efficiency with the number of QWs. Inset shows the schematic of MQWSC.

As the temperature increases from 200 to 400 K, MQWSC has exhibited ∼9.7% decrement in the value of η as compared to 11.6% in case of p-i-n solar cell. Evidently, MQWSC shows favorable results with the temperature as compared to p-i-n solar cell.

Fig. 6 displays the variation of η with the number of QWs in the intrinsic region of MQWSC. As the number of QWs increases from 10 to 20, η increases from 4.82 to 4.89%, respectively, because of the availability of more material for the low energy photons to get absorbed efficiently, which, in turn, increases η [21]. The effective increase in η tends to reduce as the number of QWs increases beyond 20. This is because of the degradation in η of photogenerated carriers from the active region due to the fading of the internal electrical field for large number of QWs [38]. Thus, it is concluded that MQWSC shows improvement in overall η as the number of QWs increases until the point where the increased absorption outweighs the increased recombination [21].

The close agreement with the published experimental data by Bae *et al.* [39], Farrell *et al.* [40], and Jeng *et al.* [41] confirms the validity of the analytical model described here. With the similar parameters of the structures as in the published literature [39]–[41], the analytical results are obtained and compared in Tables III and IV. The temperature-dependent device performance parameters are verified with those reported by Jeng *et al.* [41].

TABLE III
COMPARISON OF DEVICE PERFORMANCE PARAMETERS WITH THE EXPERIMENTAL RESULTS

Parameters	V_{ocQW} (V)	J_{scQW} (mA/cm^2)	η (%)
Bae *et al* [39]	2.20	1.25	2.30
Our Results	**2.24**	**1.43**	**2.61**
Farrel *et al* [40]	1.93	2.67	-
Our Results	**1.93**	**2.53**	**-**

TABLE IV
COMPARISON OF TEMPERATURE COEFFICIENT FOR DEVICE PERFORMANCE PARAMETERS

Temperature Coefficient	Jeng *et al* [41]	Our Results
V_{oc} (V/ °C)	-2.76×10^{-3}	$\mathbf{-2.46 \times 10^{-3}}$
J_{sc} (mA/cm^2/ °C)	0.46×10^{-3}	$\mathbf{1.0 \times 10^{-3}}$
η (%/ °C)	-9×10^{-4}	$\mathbf{-12 \times 10^{-4}}$

By comparing the results of the p-i-n and MQWs solar cell, it is clear that with the inclusion of QWs in the intrinsic region of p-i-n structure increases η as can be seen from Tables I and II, because the inclusion of QWs extends the solar cell absorption spectrum [37]. The proposed model can be used to analyze various MQWSCs based on different well and barrier materials.

IV. CONCLUSION

A physics-based generic analytical model for both the p-i-n and MQW structures is developed for the calculation of device performance parameters and obtaining J–V characteristics of the solar cell. The results show that the inclusion of QWs in the depletion region of the p-i-n solar cell leads to the enhancement of ∼27% in the conversion efficiency for the same composition ($x = 0.1$) in $In_xGa_{1-x}N$. For MQWSC, the conversion efficiency increases by ∼30% and ∼27% if the indium composition in $In_xGa_{1-x}N$ increases from $x = 0.1$ to 0.2 and further to $x = 0.3$. The temperature-dependent study of the device performance parameters has shown that, with the increase in temperature, the conversion efficiency decreases for both the solar cell. Approximately, 11.6% and 9.7% decrements in the conversion efficiency of the p-i-n and MQWSC, respectively, are obtained as the temperature increases from 200 to 400 K. The MQWSC has demonstrated more favorable temperature dependence of the efficiency compared to p-i-n solar cell. The study of the effect of the number of QWs on the solar cell has shown that the increase in the number of QWs from 10 to 20 leads to the increment in conversion efficiency from 4.28% to 4.89%. The analytical model described, and the corresponding results analyzed here can be used as a suitable model for estimating the performance parameters of MQWSC and p-i-n solar cells consisting of various material system.

ACKNOWLEDGMENT

G. Siddharth and R. Bhardwaj would like to thank MeitY for providing fellowship grant under Visvesvaraya Ph.D. Scheme.

V. Garg and B. S. Sengar would like to thank UGC and CSIR, respectively, for providing fellowship grant. S. Mukherjee would like to thank MeitY for the Young Faculty Research Fellowship (YFRF) under Visvesvaraya Ph.D. Scheme for Electronics and IT. This publication is an outcome of the Research and Development work undertaken in the project under the Visvesvaraya Ph.D. Scheme of MeitY being implemented by Digital India Corporation (formerly Media Lab Asia).

REFERENCES

[1] Y.-L. Tsai *et al.*, "Improving efficiency of InGaN/GaN multiple quantum well solar cells using CdS quantum dots and distributed Bragg reflectors," *Sol. Energy Mater. Sol. Cells*, vol. 117, pp. 531–536, Oct. 2013. doi: 10.1016/j.solmat.2013.07.004.

[2] O. Jani, I. Ferguson, C. Honsberg, and S. Kurtz, "Design and characterization of GaN/InGaN solar cells," *Appl. Phys. Lett.*, vol. 91, no. 13, Sep. 2007, Art. no. 132117. doi: 10.1063/1.2793180.

[3] O. Jani *et al.*, "Characterization and analysis of InGaN photovoltaic devices," in *Proc. 31st IEEE Photovolt. Spec. Conf.*, Jan. 2005, pp. 37–42.

[4] K. W. J. Barnham and G. Duggan, "A new approach to high-efficiency multi-band-gap solar cells," *J. Appl. Phys.*, vol. 67, no. 7, pp. 3490–3493, Apr. 1990. doi: 10.1063/1.345339.

[5] K. Barnham *et al.*, "Quantum well solar cells," *Appl. Surf. Sci.*, vols. 113–114, pp. 722–733, Apr. 1997. doi: 10.1016/S0169-4332(96)00876-8.

[6] L. Zhu *et al.*, "Diagnosis of GaInAs/GaAsP multiple quantum well solar cells with Bragg reflectors via absolute electroluminescence," *IEEE J. Photovolt.*, vol. 7, no. 3, pp. 781–786, May 2017. doi: 10.1109/JPHOTOV.2017.2662083.

[7] R. Dahal, J. Li, K. Aryal, J. Y. Lin, and H. X. Jiang, "InGaN/GaN multiple quantum well concentrator solar cells," *Appl. Phys. Lett.*, vol. 97, no. 7, Aug. 2010. Art. no. 073115. doi: 10.1063/1.3481424.

[8] J. C. Rimada, L. Hernández, J. P. Connolly, and K. W. J. Barnham, "Conversion efficiency enhancement of AlGaAs quantum well solar cells," *Microelectron. J.*, vol. 38, nos. 4–5, pp. 513–518, Apr./May 2007. doi: 10.1016/j.mejo.2007.03.007.

[9] R. Corkish and C. B. Honsberg, "Dark currents in double-heterostructure and quantum-well solar cells," in *Proc. 26th IEEE Photovolt. Spec. Conf.*, Sep./Oct. 1997, pp. 923–926. doi: 10.1109/PVSC.1997.654238.

[10] K. Xu *et al.*, "Light emission from a poly-silicon device with carrier injection engineering," *Mater. Sci. Eng. B*, vol. 231, pp. 28–31, May 2018. doi: 10.1016/j.mseb.2018.07.002.

[11] N. G. Young *et al.*, "High-performance broadband optical coatings on InGaN/GaN solar cells for multijunction device integration," *Appl. Phys. Lett.*, vol. 104, Apr. 2014, Art. no. 163902. doi: 10.1063/1.4873117.

[12] J. P. Connolly *et al.*, "Simulating multiple quantum well solar cells," in *Proc. 28th IEEE Photovolt. Spec. Conf.*, Sep. 2000 pp. 1304–1307.

[13] S. M. Ramey and R. Khoie, "Modeling of multiple-quantum-well solar cells including capture, escape, and recombination of photoexcited carriers in quantum wells," *IEEE Trans. Electron Devices*, vol. 50, no. 5, pp. 1179–1188, May 2003. doi: 10.1109/TED.2003.813475.

[14] E. Aperathitis *et al.*, "Temperature dependence of photocurrent components on enhanced performance GaAs/AlGaAs multiple quantum well solar cells," *Sol. Energy Mater. Sol. Cells*, vol. 70, no. 1, pp. 49–69, Dec. 2001. doi: 10.1016/S0927-0248(00)00411-6.

[15] N. G. Anderson, "Ideal theory of quantum well solar cells," *J. Appl. Phys.*, vol. 78, no. 3, pp. 1850–1861, Aug. 1995.break doi: 10.1063/1.360219.

[16] N. E. H. Gorji, H. Movla, F. Sohrabi, A. Hosseinpour, M. Rezaei, and H. Babaei, "The effects of recombination lifetime on efficiency and J-V characteristics of $In_xGa_{1-x}N$/GaN quantum dot intermediate band solar cell," *Phys. E, Low-Dimensional Syst. Nanostruct.*, vol. 42, no. 9, pp. 2353–2357, Jul. 2010. doi: 10.1016/j.physe.2010.05.014.

[17] A. Asgari and K. Khalili, "Temperature dependence of InGaN/GaN multiple quantum well based high efficiency solar cell," *Sol. Energy Mater. Sol. Cells*, vol. 95, no. 11, pp. 3124–3129, Nov. 2011. doi: 10.1016/j.solmat.2011.07.001.

[18] *ASTM G173-03 Reference Spectra Derived from SMARTS V.2.9.2*. Accessed: Mar. 15, 2018. [Online]. Available: https://www.nrel.gov/grid/solar-resource/spectra.html

[19] C. A. Gueymard, D. Myers, and K. Emery, "Proposed reference irradiance spectra for solar energy systems testing," *Sol. Energy*, vol. 73, no. 6, pp. 443–467, Dec. 2002. doi: 10.1016/S0038-092X(03)00005-7.

[20] M. Anani, C. Mathieu, M. Khadraoui, Z. Chama, S. Lebid, and Y. Amar, "High-grade efficiency III-nitrides semiconductor solar cell," *Microelectron. J.*, vol. 40, no. 3, pp. 427–434, Mar. 2009. doi: 10.1016/j.mejo.2008.06.008.

[21] B. W. Liou, "Design and fabrication of $In_xGa_{1-x}N$/GaN solar cells with a multiple-quantum-well structure on SiCN/Si(111) substrates," *Thin Solid Films*, vol. 520, no. 3, pp. 1084–1090, Nov. 2011. doi: 10.1016/j.tsf.2011.01.086.

[22] R. Hulstrom, R. Bird, and C. Riordan, "Spectral solar irradiance data sets for selected terrestrial conditions," *Sol. Cells*, vol. 15, no. 4, pp. 365–391, Dec. 1985. doi: 10.1016/0379-6787(85)90052-3.

[23] J. C. Rimada and L. Hernández, "Modelling of ideal AlGaAs quantum well solar cells," *Microelectron. J.*, vol. 32, no. 9, pp. 719–723, Sep. 2001. doi: 10.1016/S0026-2692(01)00058-1.

[24] T. Markvart and L. Castaner, *Solar Cells*. Amsterdam, The Netherlands: Elsevier, 2005, p. 34.

[25] M. A. Green, *Solar Cells: Operating Principles, Technology, and System Applications*. Upper Saddle River, NJ, USA: Prentice-Hall, 1982, p. 80.

[26] S. R. Kurtz, P. Faine, and J. M. Olson, "Modeling of two-junction, series-connected tandem solar cells using top-cell thickness as an adjustable parameter," *J. Appl. Phys.*, vol. 68, no. 4, pp. 1890–1895, Aug. 1990. doi: 10.1063/1.347177.

[27] H. Sun *et al.*, "A dependency of emission efficiency of poly-silicon light-emitting device on avalanching current," *Opt. Mater.*, vol. 88, pp. 711–717, Feb. 2019. doi: 10.1016/j.optmat.2018.12.013.

[28] H. Elghazi, A. Jorio, and I. Zorkani, "Analysis of temperature and 1 MeV proton irradiation effects on the light emission in bulk silicon (npn) emitter-base bipolar junctions," *Opt. Commun.*, vol. 280, no. 2, pp. 278–284, Dec. 2007. doi: 10.1016/j.optcom.2007.08.058.

[29] J. Wu *et al.*, "Small band gap bowing in $In_{1-x}Ga_xN$ alloys," *Appl. Phys. Lett.*, vol. 80, no. 25, pp. 4741–4743, Jun. 2002. doi: 10.1063/1.1489481.

[30] Y. P. Varshni, "Temperature dependence of the energy gap in semiconductors," *Physica*, vol. 34, no. 1, pp. 149–154, 1967. doi: 10.1016/0031-8914(67)90062-6.

[31] H. Haug and S. W. Koch, *Quantum Theory of the Optical and Electronic Properties of Semiconductors*. Singapore: World Scientific, 2009, p. 83.

[32] P. Wurfel and U. Wurfel, *Physics of Solar Cells: From Basic Principles to Advanced Concepts*. Hoboken, NJ, USA: Wiley, 2016, p. 182.

[33] K. Xu, "Monolithically integrated Si gate-controlled light-emitting device: Science and properties," *J. Opt.*, vol. 20, no. 2, Jan. 2018, Art. no. 024014. doi: 10.1088/2040-8986/aaa2b7.

[34] V. Garg, B. S. Sengar, A. Kumar, G. Siddharth, S. Kumar, and S. Mukherjee, "Investigation of valence plasmon excitations in GMZO thin film and their suitability for plasmon-enhanced buffer-less solar cells," *Sol. Energy*, vol. 178, pp. 114–124, Jan. 2019. doi: 10.1016/j.solener.2018.12.017.

[35] J. Wong *et al.*, "Lifetime limiting recombination pathway in thin-film polycrystalline silicon on glass solar cells," *J. Appl. Phys.*, vol. 107, no. 12, Jun. 2010, Art. no. 123705. doi: 10.1063/1.3429206.

[36] Z. Chen *et al.*, "Positive temperature coefficient of photovoltaic efficiency in solar cells based on InGaN/GaN MQWs," *Appl. Phys. Lett.*, vol. 109, no. 6, Aug. 2016, Art. no. 062104. doi: 10.1063/1.4960765.

[37] B. W. Liou, "Temperature of $In_xGa_{1-x}N$/GaN solar cells with a multiple-quantum-well structure on SiCN/Si(111)substrates," *Sol. Energy Mater. Sol. Cells*, vol. 114, pp. 141–146, Jul. 2013. doi: 10.1016/j.solmat.2013.02.014.

[38] T. Inoue, K. Watanabe, K. Toprasertpong, H. Fujii, M. Sugiyama, and Y. Nakano, "Enhanced light trapping in multiple quantum wells by thin-film structure and backside grooves with dielectric interface," *IEEE J. Photovolt.*, vol. 5, no. 2, pp. 697–703, Mar. 2015. doi: 10.1109/JPHOTOV.2015.2392941.

[39] S.-Y. Bae, J.-P. Shim, D.-S. Lee, S.-R. Jeon, and G. Namkoong, "Improved photovoltaic effects of a vertical-type InGaN/GaN multiple quantum well solar cell," *Jpn. J. Appl. Phys.*, vol. 50, no. 9R, Sep. 2011, Art. no. 092301. doi: 10.1143/JJAP.50.092301.

[40] R. M. Farrell *et al.*, "High quantum efficiency InGaN/GaN multiple quantum well solar cells with spectral response extending out to 520 nm," *Appl. Phys. Lett.*, vol. 98, no. 20, May 2011, Art. no. 201107. doi: 10.1063/1.3591976.

[41] M.-J. Jeng, Y.-L. Lee, and L.-B. Chang, "Temperature dependences of $In_xGa_{1-x}N$ multiple quantum well solar cells," *J. Phys. D, Appl. Phys.*, vol. 42, no. 10, Apr. 2009, Art. no. 105101. doi: 10.1088/0022-3727/42/10/105101.